Received: 18 February 2022 | Revised: 03 September 2022 | Accepted: 09 September 2022

DOI: 10.1002/hep.32782

ORIGINAL ARTICLE

OPEN

$CD11b^{+}CD43^{hi}Ly6C^{lo}$ splenocyte-derived macrophages exacerbate liver fibrosis via spleen–liver axis

Shaoying Zhang[1,2,3] | Dan Wan[1,2,3] | Mengchen Zhu[1,2,3] | Guihu Wang[1,2,3] | Xurui Zhang[1,2,3] | Na Huang[1,2] | Jian Zhang[1,2] | Chongyu Zhang[1,2,3] | Qi Shang[1,2,3] | Chen Zhang[1,2,3] | Xi Liu[1,2,3] | Fanfan Liang[1,2,3] | Chunyan Zhang[1] | Guangyao Kong[1,2] | Jing Geng[1,3] | Libo Yao[1] | Shemin Lu[1,3,4] | Yongyan Chen[5,6] | Zongfang Li[1,2,3,4]

[1]National-Local Joint Engineering Research Center of Biodiagnosis & Biotherapy, The Second Affiliated Hospital, Xi'an Jiaotong University, Xi'an, China

[2]Shaanxi Provincial Clinical Medical Research Center for Liver and Spleen Diseases, CHESS-Shaanxi consortium, The Second Affiliated Hospital, Xi'an Jiaotong University, Xi'an, China

[3]Shaanxi International Cooperation Base for Inflammation and Immunity, Xi'an, China

[4]Key Laboratory of Environment and Genes Related to Diseases, Xi'an Jiaotong University, Ministry of Education of China, Xi'an, China

[5]Hefei National Laboratory for Physical Sciences at Microscale, the CAS Key Laboratory of Innate Immunity and Chronic Disease, School of Basic Medical Sciences, Division of Life Sciences and Medicine, University of Science and Technology of China, Hefei, China

[6]Institute of Immunology, University of Science and Technology of China, Hefei, China

Correspondence
Shemin Lu, National-Local Joint Engineering Research Center of Biodiagnosis & Biotherapy, The Second Affiliated Hospital, Xi'an Jiaotong University, No.157, Xiwu Rd, Xi'an, 710004, China.
Email: lushemin@xjtu.edu.cn

Yongyan Chen, Hefei National Laboratory for Physical Sciences at Microscale, the CAS Key Laboratory of Innate Immunity and Chronic Disease, School of Basic Medical Sciences, Division of Life Sciences and Medicine, University of Science and Technology of China, Huangshan Rd 443, Hefei, 230027, China.
Email: yychen08@ustc.edu.cn

Zongfang Li, National-Local Joint Engineering Research Center of Biodiagnosis & Biotherapy, The Second Affiliated Hospital, Xi'an Jiaotong University, No.157, Xiwu Rd, Xi'an, 710004, China.
Email: lizongfang@xjtu.edu.cn

Abstract

Background and Aims: Monocyte-derived macrophages (MoMFs), a dominant population of hepatic macrophages under inflammation, play a crucial role in liver fibrosis progression. The spleen serves as an extra monocyte reservoir in inflammatory conditions; however, the precise mechanisms of involvement of the spleen in the pathogenesis of liver fibrosis remain unclear.

Approach and Results: By splenectomy and splenocyte transfusion, it was observed that splenic $CD11b^{+}$ cells accumulated intrahepatically as $Ly6C^{lo}$ MoMFs to exacerbate CCl_4-induced liver fibrosis. The splenocyte migration into the fibrotic liver was further directly visualized by spleen-specific photoconversion with KikGR mice and confirmed by $CD45.1^{+}/CD45.2^{+}$ spleen transplantation. Spleen-derived $CD11b^{+}$ cells purified from fibrotic livers were then annotated by single-cell RNA sequencing, and a subtype of $CD11b^{+}CD43^{hi}Ly6C^{lo}$ splenic monocytes (sM-1s) was identified, which was

Abbreviations: FSDM, fibrotic spleen-derived myeloid cell; HSC, hepatic stellate cell; KikGR, Kikume Green-Red; liver-CM, fibrotic hepatocyte conditioned medium; MoMF, monocyte-derived macrophage; Mono, monocyte/macrophage; ROS, reactive oxygen species; sM, spleen-derived monocyte; sMφ, spleen-derived macrophage; SP^{-}, without spleen; WD-HFD, Western high-fat diet.

Supplemental Digital Content is available for this article. Direct URL citations appear in the printed text and are provided in the HTML and PDF versions of this article on the journal's website, www.hepjournal.com.

Funding information
National Natural Science Foundation of China, Grant/Award Number: 91842307, 82101915, 82173207 and 81922003; Natural Science Foundation of Shaanxi Province, Grant/Award Number: 2019JQ-970; Innovation Capacity Support Plan of Shaanxi Province, Grant/Award Number: S2020-ZC-GHJD-0012

markedly expanded in both spleens and livers of mice with liver fibrosis. sM-1s exhibited mature feature with high expressions of F4/80, produced much ROS, and manifested preferential migration into livers. Once recruited, sM-1s underwent sequential transformation to sM-2s (highly expressed *Mif*, *Msr1*, *Clec4d*, and *Cstb*) and then to spleen-derived macrophages (sMφs) with macrophage features of higher expressions of CX_3CR1, F4/80, MHC class II, and CD64 in the fibrotic hepatic milieu. Furthermore, sM-2s and sMφs were demonstrated capable of activating hepatic stellate cells and thus exacerbating liver fibrosis.

Conclusions: $CD11b^+CD43^{hi}Ly6C^{lo}$ splenic monocytes migrate into the liver and shift to macrophages, which account for the exacerbation of liver fibrosis. These findings reveal precise mechanisms of spleen–liver axis in hepatic pathogenesis and shed light on the potential of sM-1 as candidate target for controlling liver diseases.

INTRODUCTION

Liver fibrosis is an outcome of liver injury hallmarked by excessive accumulation of extracellular matrix (ECM) produced by activated and transdifferentiated hepatic stellate cells (HSCs). Fibrogenesis is often preceded by chronic inflammation,[1,2] and durable inflammation further triggers the development of cirrhosis and even hepatocellular carcinoma.[3] In response to the inflammatory signals, activated immune cells are recruited to the injured liver, helping maintain the inflammatory hepatic environment and, thus, facilitate the progression of liver diseases.[4,5] Emerging evidence suggests the spleen as an extra inflammatory cell resource beyond bone marrow in certain liver diseases, based on the results that the spleen affects the composition of hepatic immune cells.[6–9] However, the precise mechanisms of involvement of the spleen in the pathogenesis of liver fibrosis have not been well understood.

The spleen and liver are both involved in immune response and connected anatomically and physiologically. All splenic blood flows into the liver through the portal vein. Pathologically, liver cirrhosis with portal hypertension often manifests with splenomegaly and hypersplenism. Changes in splenic blood microcirculation and spleen stiffness are capable of evaluating portal hypertension.[10,11] Clinically, splenectomy ameliorates patients' condition.[12–14] Moreover, a spleen–liver axis has been defined to describe the crosstalk between the spleen and liver.[15–17] Spleen-derived cytokines including transforming growth factor-β1 (TGF-β1), IL-10, and TNF,[18–20] chemokine like CCL2,[21] and factors involved in metabolic activities[16,22] have been shown to play essential roles in linking the spleen and liver.[23] Yet, little evidence is provided for splenocytes acting as mediators of the spleen–liver axis, although a few studies in liver diseases have demonstrated altered composition of hepatic immune cells upon splenectomy.[6–9,24] Therefore, the response of splenocytes to liver inflammatory signals and the use of cell tracing technology to study splenocyte migration deserve further investigation to understand the pathogenesis of the spleen–liver axis in liver diseases.

Macrophages are the most abundant immune cells in the liver, playing critical roles in liver inflammation. Liver macrophages include liver-resident macrophages (Kupffer cells) and monocyte-derived macrophages (MoMFs),[25–27] and the latter are the major players during liver inflammation. MoMFs play a proinflammatory and profibrotic role by activating themselves,[28–30] helping recruit leukocytes and HSCs, and establishing crosstalk with other cells.[31–34] Bone marrow has long been considered the only source of circulating monocytes[35]; however, the spleen has lately been proven to serve as a monocyte reservoir to accommodate the demands of rapid-onset inflammation in conditions such as ischemic myocardial injury, ischemic brain injury, atherosclerotic lesions, and hepatopulmonary syndrome.[36–40] Therefore, exploration of the response of splenic monocytes in inflammatory liver diseases has predictable significance.

In this study, by using mouse models of liver fibrosis induced by both CCl_4 and a Western high-fat diet (WD-HFD), a subtype of spleen-derived monocytes identified as $CD11b^+CD43^{hi}Ly6C^{lo}$ cells are demonstrated to preferentially recruit into fibrotic liver and acquire macrophage features to exacerbate fibrogenesis. These findings provide strong evidence for the critical role of the spleen–liver axis in the progression of chronic liver disease.

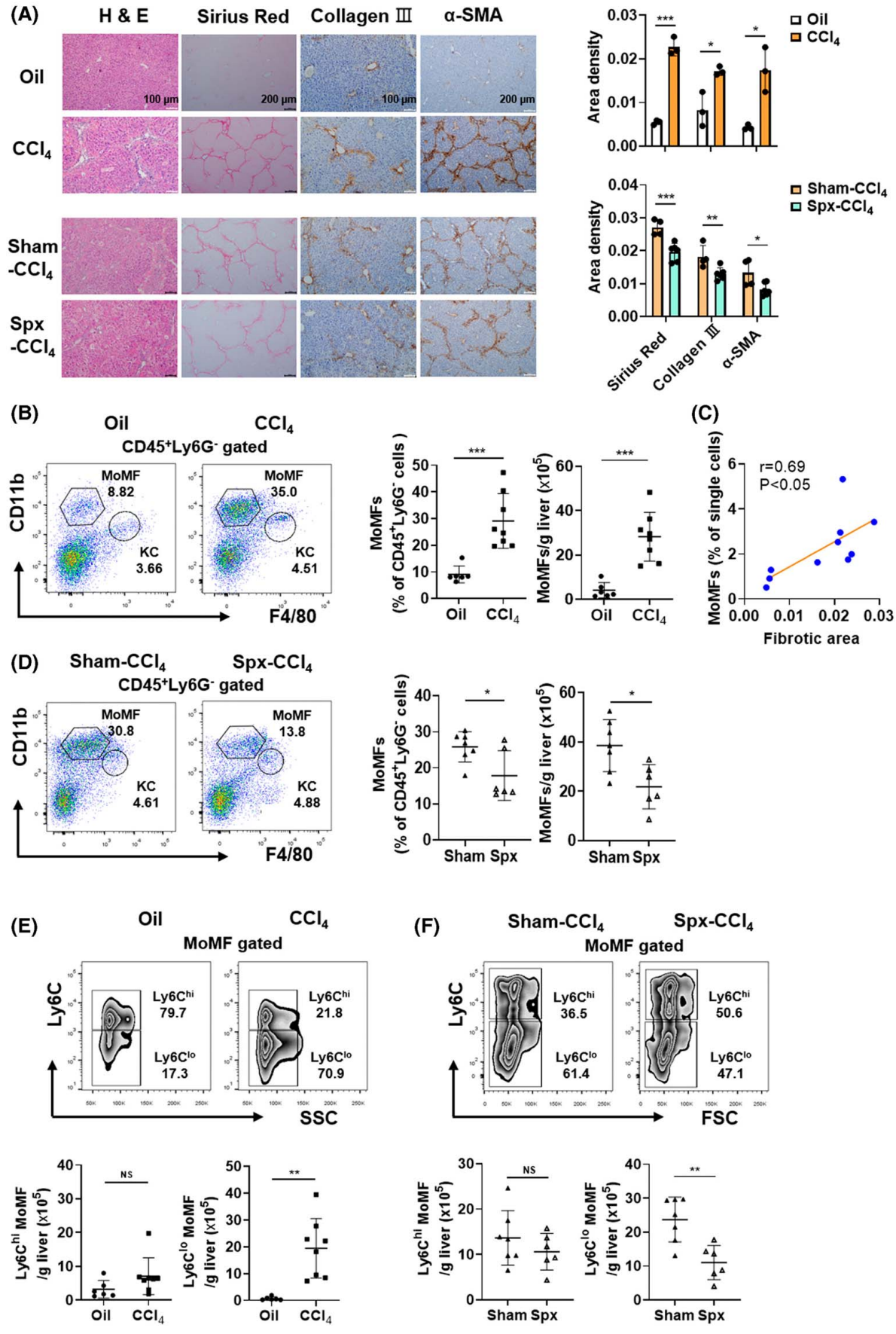
(A)
H & E
Sirius Red
Collagen Ⅲ
α-SMA
Oil
CCl4
Sham-CCl4
Spx-CCl4
100 μm
200 μm
Area density
Oil
CCl4
Sham-CCl4
Spx-CCl4
Sirius Red
Collagen Ⅲ
α-SMA
(B)
CD45+Ly6G- gated
CD11b
F4/80
MoMF 8.82
KC 3.66
MoMF 35.0
KC 4.51
MoMFs (% of CD45+Ly6G- cells)
MoMFs/g liver (x10^5)
(C)
r=0.69
P<0.05
MoMFs (% of single cells)
Fibrotic area
(D)
MoMF 30.8
KC 4.61
MoMF 13.8
KC 4.88
(E)
MoMF gated
Ly6C
SSC
Ly6Chi 79.7
Ly6Clo 17.3
Ly6Chi 21.8
Ly6Clo 70.9
Ly6Chi MoMF /g liver (x10^5)
Ly6Clo MoMF /g liver (x10^5)
NS
(F)
FSC
Ly6Chi 36.5
Ly6Clo 61.4
Ly6Chi 50.6
Ly6Clo 47.1

FIGURE 1 Spleen facilitates intrahepatic accumulation of Ly6C^{lo} monocyte-derived macrophages (MoMFs) to exacerbate liver fibrosis. (A) Representative histological images of hematoxylin and eosin (H&E), Sirius Red, collagen III, and α-smooth muscle actin (α-SMA) staining in formalin-fixed and paraffin-embedded liver tissue from mice treated with oil or CCl_4, and quantification of positive area fraction. Scale bar, 100 μm (H&E and α-SMA) or 200 μm (Sirius Red and collagen III). (B) Representative cytometry for gating MoMFs (CD45$^+$Ly6G$^-$CD11b^{hi}F4/80^{int}) from livers of mice treated with oil or CCl_4. Frequencies and absolute numbers of MoMFs were then calculated. (C) Correlation analysis of hepatic MoMF frequency and fibrotic area. (D) Representative cytometry for gating MoMFs from livers of sham-operated (Sham) or splenectomy (Spx) mice treated with CCl_4. Frequencies and absolute numbers of MoMFs were then calculated. (E) Representative cytometry of Ly6C expression on hepatic MoMFs of mice treated with oil or CCl_4. Absolute numbers of Ly6C^{hi} and Ly6C^{lo} MoMFs were then calculated. (F) Representative cytometry of Ly6C expression on hepatic MoMFs of Sham or Spx mice. Absolute numbers of Ly6C^{hi} and Ly6C^{lo} MoMFs were then calculated. Data are shown as the mean ± SEM. Regression analysis and the Student's *t* test are performed for statistical significance. *, **, and *** stand for $p < 0.05$, <0.01, and <0.001, respectively.

MATERIALS AND METHODS

Mice

Adult male C57BL/6 mice aged 6–8 weeks were purchased from GemPharmatech Co., Ltd. B6. Cg-*Gt(ROSA)26Sor* < *tm1.1(CAG-kikGR)Kgwa* > (Riken BRC 09256, referred to as KikGR) mice were purchased from Riken BRC Experimental Animal Division. B6.SJL-*Ptprc*^{a} *Pepc*^{b}/BoyJ (no. 002014, referred to as CD45.1$^+$) mice were purchased from the Jackson Laboratory. All mice were maintained under specific pathogen-free controlled conditions and received humane care according to the criteria outlined in the NIH Guide for the Care and Use of Laboratory Animals.

Mouse models

Liver fibrosis was induced by intraperitoneal injection of 0.4 μl g^{-1} body weight CCl_4 (Sigma-Aldrich) diluted 1:3 in olive oil twice a week for 6 weeks, and control mice were given olive oil. Otherwise, mice were fed with a WD-HFD (with 60 kcal% fat) to induce NAFLD or a corresponding control diet for 10 weeks.

Patients

Liver samples were obtained from patients with hepatitis B cirrhosis-related portal hypertension complicated with hypersplenism. These patients underwent a splenectomy and liver biopsy at The Second Affiliated Hospital of Xi'an Jiaotong University. Details on patient information are provided in Table S3.

Cell

The mouse HSC line *JS1* was a gift from Jinsheng Guo of Department of Gastroenterology and Hepatology, Zhongshan Hospital (Fudan University, China) and cultured as described previously.[41,42]

KikGR photoconversion and intravital microscopy

KikGR transgenic mice were anesthetized with isoflurane (Sigma-Aldrich) supplemented with oxygen (1%–3% vol, by inhalation), and the spleen was externalized gently, with two pieces of sterile aluminum foil arranged on either side of the spleen, shielding the skin and abdominal cavity. Then the spleen was irradiated 5 min/field with short wavelength laser light (405 nm) laser under a compound microscope (Zeiss, Germany) equipped with 5× objective. After photoconversion, the spleen was replaced, and the abdominal cavity and skin were closed. Twenty-four hours after photoconversion, the mice were anesthetized and placed within a custom-designed box, with the liver exposed for imaging. Imaging was performed on an inverted TCS SP8 laser scanning confocal microscope (Leica).

Spleen transplantation

Spleen donor mice (CD45.1$^+$ or KikGR) were anesthetized and intravenously injected with heparin. The thorax was opened, and the right atrium was incised to allow blood to flow out during perfusion. Then, the donor spleen containing the splenic artery and splenic vein was removed and stored in ice cold heparin-saline. The spleen of the anesthetized recipient (CD45.2$^+$) was removed after ligation of the splenic vein and artery at the splenic hilar. After that, the donor spleen was placed at the right flank of recipient abdomen without twists. End-to-side anastomosis was performed on the donor's portal vein to the recipient's portal vein, as well as donor's aortic cuff to the recipient's infrarenal aorta. The abdominal cavity and skin were closed.

Single-cell RNA sequencing

The viable CD11b$^+$ cells were isolated and subjected to single-cell RNA sequencing (scRNA-seq) analysis using the Chromium microfluidic chips with 30 v3 Chemistry and barcoded with a 10× Chromium Controller (10X Genomics). RNA from the barcoded

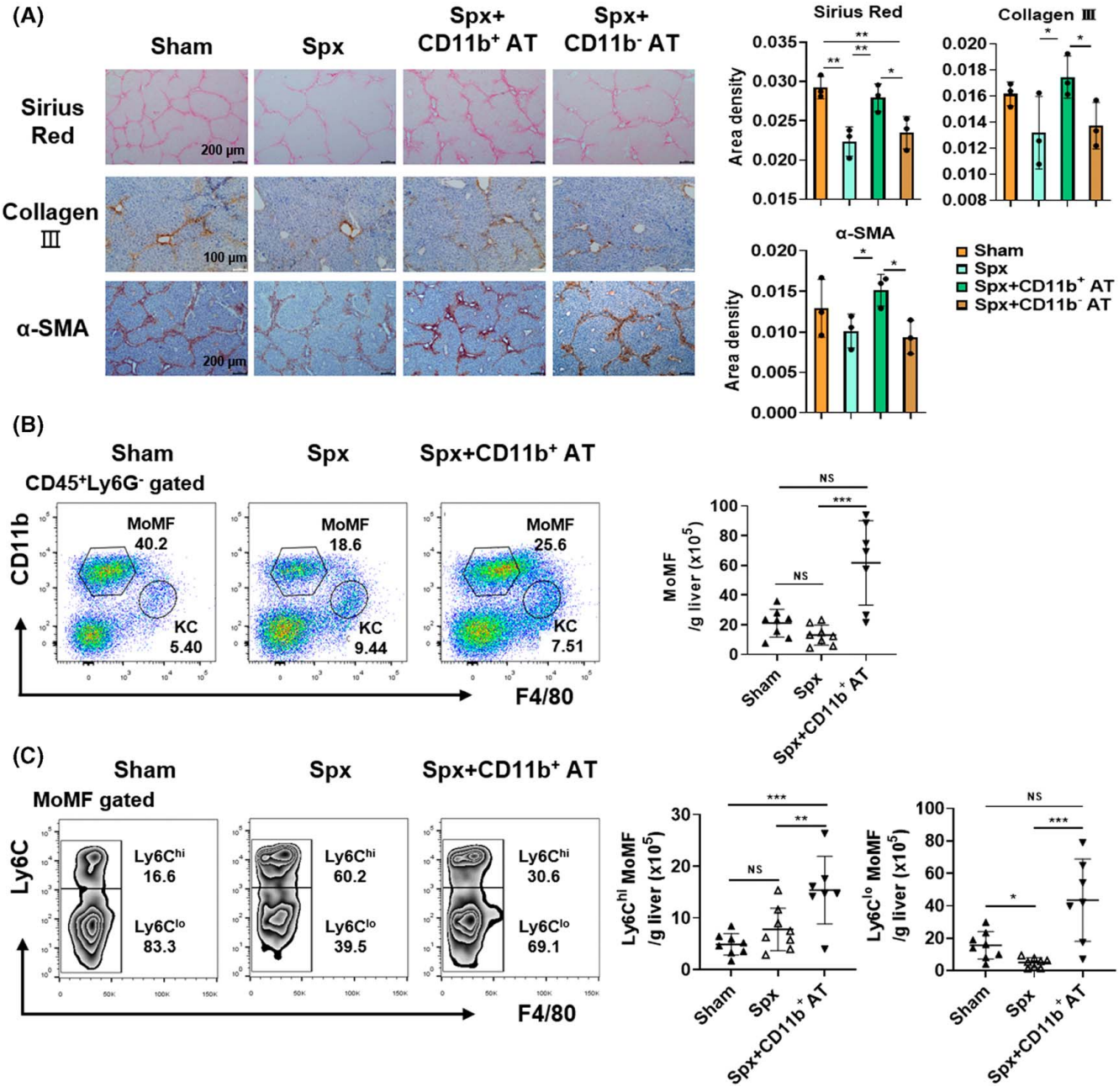

FIGURE 2 Splenic CD11b+ cells accumulate Ly6C^{lo} monocyte-derived macrophages (MoMFs) to exacerbate liver fibrosis. (A) Representative histological images of Sirius Red, collagen III, and α-SMA staining in formalin-fixed and paraffin-embedded liver tissues, and quantification of positive area fraction. Scale bar, 100 μm (collagen III and α-SMA) or 200 μm (Sirius Red). (B) Representative cytometry for gating MoMFs from livers of mice treated with CCl_4 that underwent different operations. Absolute numbers of MoMFs were then calculated. (C) Representative cytometry of Ly6C expression on hepatic MoMFs. Absolute numbers of Ly6C^{hi} and Ly6C^{lo} MoMFs were then calculated. Male C57BL/6 mice intraperitoneally injected with CCl_4 for 6 weeks were divided into four groups and underwent sham operation (Sham), splenectomy (Spx), or adoptive transfusion (AT) with splenic CD11b$^+$ or CD11b cells 2 weeks after Spx (Spx+CD11b$^+$AT or Spx+CD11b$^-$AT), respectively. Data are shown as the mean ± SEM. One-way analysis of variance (ANOVA) and multiple comparisons (LSD) after ANOVA were performed for statistical significance. *, ** and, *** stand for $p < 0.05$, <0.01, and <0.001, respectively.

cells was subsequently reverse-transcribed and sequencing libraries were constructed with reagents from a Chromium Single Cell 30 v3 reagent kit (10X Genomics) according to the manufacturer's instructions. Sequencing was performed with Illumina NovaSeq according to the manufacturer's instructions (Illumina).

scRNA-seq data analysis

Raw fastqs were mapped to genome reference consortium mouse build 38 organism to generate count matrix by the Cell Ranger software (v4.0). Downstream analysis was performed by R package Seurat (v3.0.2), including quality control, principal component analysis,

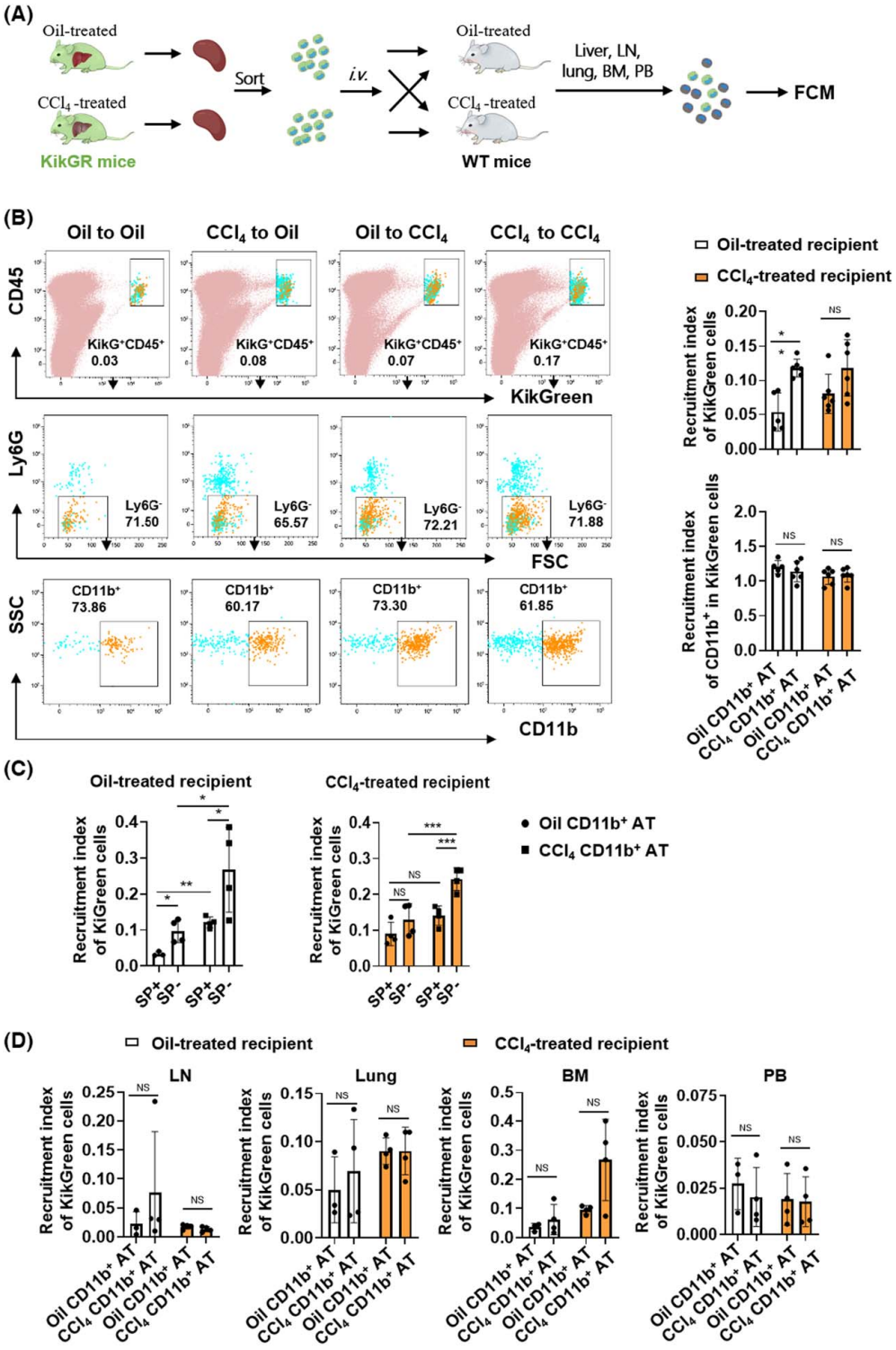

FIGURE 3 Splenic CD11b$^+$ cells from mice with liver fibrosis manifest advantageous migration into liver. (A) Scheme of splenic cell adoptive transfusion assays. A total of 1×10^6 splenic CD11b$^+$ cells sorted from either Oil- or CCl_4-treated KikGR mice were adoptively transferred to Oil- or CCl_4-treated wild-type (WT) mice, repeatedly. KikGreen cells (KikG+) migrated to the recipient livers were detected by flow cytometry 24 h later. In some experiments (D), spleens of the recipient mice were removed 2 weeks before cell transfusion. (B) Representative cytometry for gating transfused splenic KikG$^+$CD11b$^+$ cells in livers of recipient mice. Recruitment index of transfused KikG$^+$ cells in liver single cells and CD11b$^+$ cells in KikG$^+$ cells. (C) Recruitment index of transfused KikG$^+$ cells in livers of recipients with (SP+) or without spleen (SP−). (D) Recruitment index of transfused KikG+ cells in lymph node (LN), lung, bone marrow (BM), and peripheral blood (PB). Recruitment index: frequency of target cells in the recipient liver / frequency of target cells in transfused splenic cells. Data are shown as the mean ± SEM. Mann–Whitney rank sum test and the Student's *t* test were performed for statistical significance. *, **, and *** stand for $p < 0.05$, <0.01, and <0.001, respectively. FCM, flow cytometry; i.v., intravenous injection; NS, no significance.

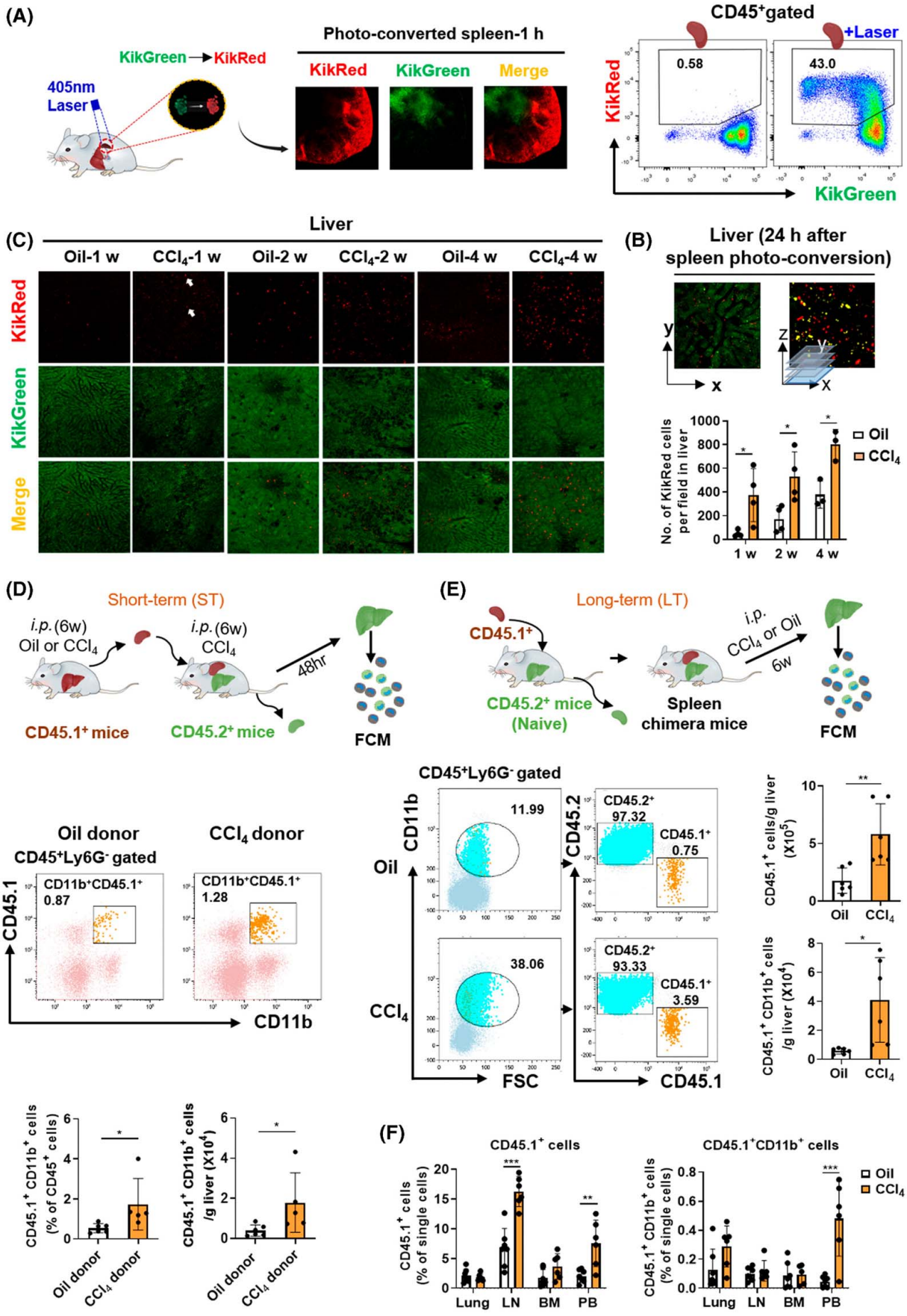
(A)
KikGreen → KikRed
405nm Laser
Photo-converted spleen-1 h
KikRed
KikGreen
Merge
CD45+gated
+Laser
0.58
43.0
KikRed
KikGreen
(C)
Liver
Oil-1 w
CCl4-1 w
Oil-2 w
CCl4-2 w
Oil-4 w
CCl4-4 w
KikRed
KikGreen
Merge
(B)
Liver (24 h after spleen photo-conversion)
No. of KikRed cells per field in liver
Oil
CCl4
1 w
2 w
4 w
(D)
Short-term (ST)
i.p. (6w) Oil or CCl4
i.p. (6w) CCl4
48hr
CD45.1+ mice
CD45.2+ mice
FCM
(E)
Long-term (LT)
CD45.1+
CD45.2+ mice (Naive)
Spleen chimera mice
i.p. CCl4 or Oil
6w
FCM
Oil donor
CCl4 donor
CD45+Ly6G- gated
CD11b+CD45.1+ 0.87
CD11b+CD45.1+ 1.28
CD45.1
CD11b
CD45+Ly6G- gated
CD11b
CD45.2
Oil
CCl4
11.99
CD45.2+ 97.32
CD45.1+ 0.75
38.06
CD45.2+ 93.33
CD45.1+ 3.59
FSC
CD45.1
CD45.1+ cells/g liver (X10^5)
CD45.1+ CD11b+ cells /g liver (X10^4)
Oil
CCl4
CD45.1+ CD11b+ cells (% of CD45+ cells)
CD45.1+ CD11b+ cells /g liver (X10^4)
Oil donor
CCl4 donor
(F)
CD45.1+ cells
CD45.1+CD11b+ cells
CD45.1+ cells (% of single cells)
CD45.1+ CD11b+ cells (% of single cells)
Lung
LN
BM
PB
Oil
CCl4

FIGURE 4 Splenic CD11b$^+$ cells are visualized to accumulate intrahepatically in mice with liver fibrosis. (A) Imaging of photoconverted spleen, and representative cytometry for photoconversion efficiency of splenocytes. (B) Representative two-photon in vivo imaging of livers of mice received spleen-specific photoconversion. (C) Representative imaging of livers of mice undergoing different treatments followed by spleen-specific photoconversion. KikRed$^+$ splenocytes in livers were then counted. (D) Short-term (ST) spleen transplantation experiment. Representative cytometry for gating donor spleen-derived CD45.1$^+$Ly6G$^-$CD11b$^+$ cells in livers of ST spleen transplantation mice. Frequencies of the cells in hepatic CD45$^+$ cells and absolute numbers of the cells in livers were then calculated. (E) Long-term (LT) spleen transplantation experiment. Representative cytometry for gating donor spleen-derived CD45.1$^+$Ly6G$^-$CD11b$^+$ cells in livers of LT spleen transplantation mice. Absolute numbers of CD45.1$^+$ and CD45.1$^+$Ly6G$^-$CD11b$^+$ cells in livers were then calculated. (F) Frequencies of donor spleen-derived CD45.1$^+$ cells and CD45.1$^+$Ly6G$^-$CD11b$^+$ cells in single cells of lung, lymph node (LN), bone marrow (BM), and peripheral blood (PB). Data are shown as the mean ± SEM. Student's *t* test was performed for statistical significance. *, **. and *** stand for $p < 0.05$, <0.01, and <0.001, respectively. CCl4-1w, mice treated with CCl4 for one week; FCM, flow cytometry; i.p., intraperitoneal; Oil-1w, mice treated with oil for one week.

t-distributed stochastic neighbor embedding, or Uniform Manifold Approximation and Projection dimension reduction and clustering. Cells with more than 500 genes and less than 8000 genes, and with less than 10% unique molecular identifiers (UMIs) derived from the mitochondrial genes, were retained for downstream analysis. Thirty components and 0.5 resolution were used in reduction and clustering, respectively; other parameters in each step were ran with the default value. Candidate cluster markers were calculated by function Find All Markers in Seurat. Genes from each cluster with average log fold change ≥ 0.5 and adjusted p value ≤ 0.05 were used as input gene sets for kyoto encyclopedia of genes and genomes (KEGG) and gene ontology (GO) enrichment analysis in R package Cluster Profiler (v3.12.0). RNA velocity was estimated by R package velocyto.R (v0.6) to infer the cell trajectory.

Statistical analysis

All data are shown as mean ± SEM. Student's *t* test, one-way analysis of variance (ANOVA) and further least significant difference (LSD) for multiple comparisons, and Mann–Whitney rank sum test were performed for the statistical significance among groups. Regressive analysis was run for significance of correlation. $p < 0.05$ is considered to be statistically significant.

Statement

All animal experiments were ethically approved by the Animal Use and Management Committee of the Xi'an Jiaotong University of China. All research involving human samples was conducted in accordance with both the Declarations of Helsinki and Istanbul. All participants provided written informed consent. All procedures were approved by the Ethics Committee of The Second Affiliated Hospital of Xi'an Jiaotong University of China (no. 2018479).

RESULTS

Splenic CD11b$^+$ cells accumulate intrahepatically as Ly6C^{lo} MoMFs to facilitate liver fibrosis progression

Compared with Oil-treated mice, mice treated with CCl_4 showed obvious liver fibrosis with increased levels of collagen III and α-smooth muscle actin (α-SMA) deposition, whereas splenectomy markedly reduced the deposition (Figure 1A). Along with fibrogenesis, MoMFs marked by CD11b^{hi}F4/80^{int} accumulated in livers (Figure 1B). The frequency of MoMFs showed close correlation with the fibrosis area (Figure 1C), and accumulation of MoMFs was impaired upon spleen removal (Figure 1D). Moreover, the accumulated MoMFs in livers of CCl_4-treated mice were mainly composed of the Ly6C^{lo} group (Figure 1E), which also significantly decreased in splenectomy mice (Figure 1F). These findings suggest the spleen be responsible for the accumulated MoMFs, especially the Ly6C^{lo} ones in fibrotic liver, and thus exacerbate the progression of liver fibrosis.

To verify the candidate cells that account for the role of spleen in liver fibrosis, splenic CD11b$^+$ or CD11b$^-$ cells were transfused to splenectomy mice. Compared with the splenectomy mice, mice receiving the transfusion CD11b$^+$ cells, but not CD11b$^-$ cells, showed exacerbated liver fibrosis (Figure 2A, Figure S1A). Also, CD11b$^+$ cell transfusion facilitated the accumulation of mainly Ly6C^{lo} MoMFs and a few Ly6C^{hi} ones (Figure 2B,C), and this was independent of the cell sourcing from Oil- or CCl_4-treated mice (Figure S1B.

Migration of splenic CD11b$^+$ cells to the liver was confirmed by cell transfusion and tracking (Figure 3A). While being transfused to Oil-treated recipients, splenic CD11b$^+$ cells from CCl_4-treated mice showed significant migration advantage to livers than cells from Oil-treated mice, but the advantage was faded in CCl_4-treated recipients (Figure 3B). In consideration of the possible competitive migration of splenic cells from CCl_4-treated recipients with the donor cells, cell transfusion was further performed in recipients with spleen (SP$^+$) or without spleen (SP$^-$). In Oil-treated recipients, splenic CD11b$^+$

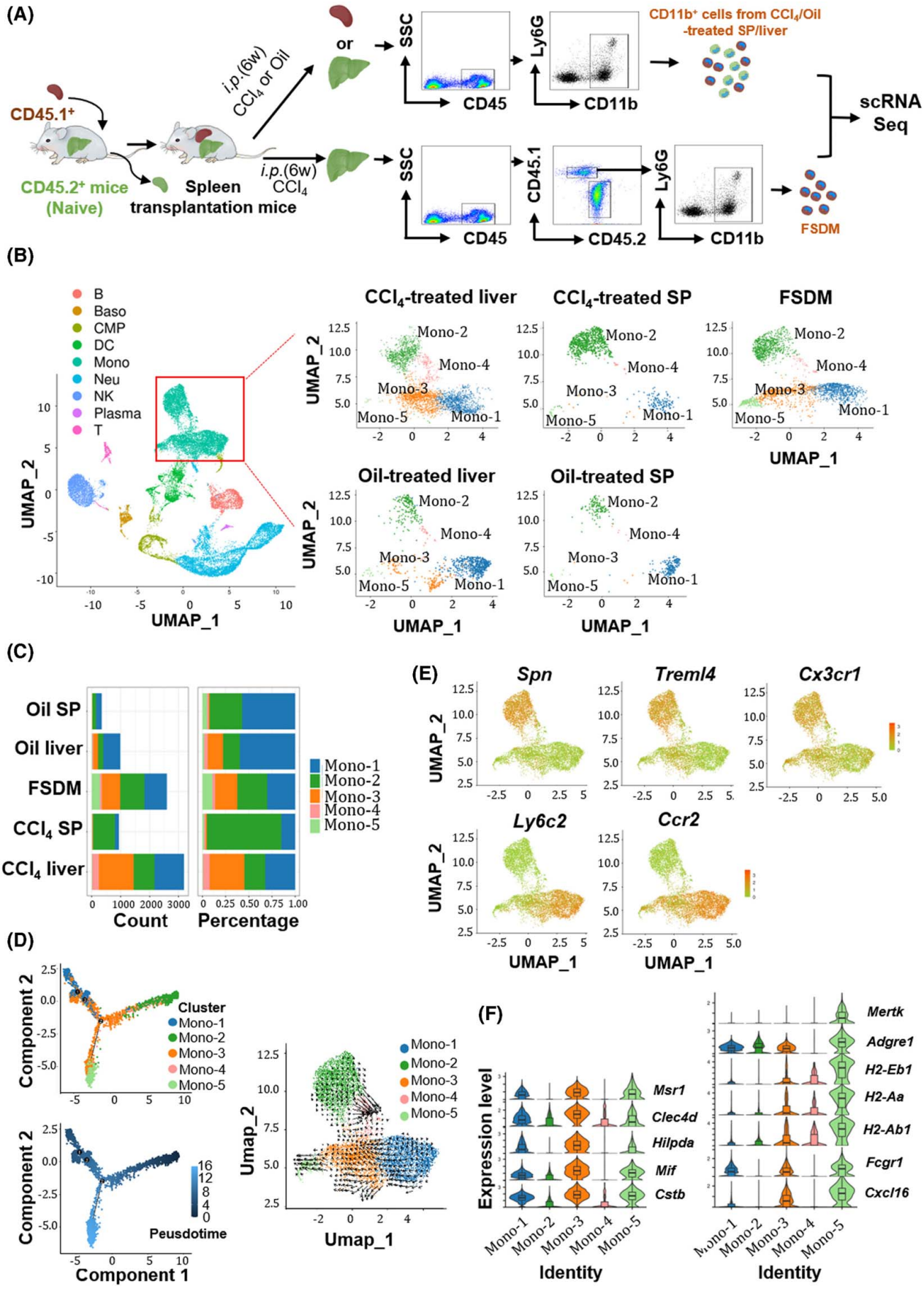
(A)
CD45.1+
CD45.2+ mice
(Naive)
Spleen
transplantation mice
i.p.(6w)
CCl4 or Oil
i.p.(6w)
CCl4
or
SSC
CD45
Ly6G
CD11b
CD11b+ cells from CCl4/Oil
-treated SP/liver
scRNA
Seq
CD45.1
CD45.2
FSDM
(B)
B
Baso
CMP
DC
Mono
Neu
NK
Plasma
T
UMAP_1
UMAP_2
CCl4-treated liver
CCl4-treated SP
FSDM
Oil-treated liver
Oil-treated SP
Mono-1
Mono-2
Mono-3
Mono-4
Mono-5
(C)
Oil SP
Oil liver
FSDM
CCl4 SP
CCl4 liver
Count
Percentage
(D)
Component 1
Component 2
Cluster
Peusdotime
Umap_1
Umap_2
(E)
Spn
Treml4
Cx3cr1
Ly6c2
Ccr2
(F)
Expression level
Msr1
Clec4d
Hilpda
Mif
Cstb
Mertk
Adgre1
H2-Eb1
H2-Aa
H2-Ab1
Fcgr1
Cxcl16
Identity

FIGURE 5 Specific monocyte/macrophage subtypes derived from splenic CD11b$^+$ cells are identified in fibrotic livers (A) Scheme of cell isolation, and single-cell RNA sequencing (scRNA-seq) of CD11b$^+$ myeloid cells from indicated samples. Five cell samples were prepared for scRNA-seq as follows: spleen and liver CD11b$^+$ cells were sorted from pools of three Oil-treated or three CCl_4-treated mice, and corresponding spleen and liver cells were derived from the same mice; the fibrotic spleen-derived myeloid cells (FSDMs) were CD45.1$^+$CD11b$^+$ cells isolated from a mixture of liver cells from nine CCl_4-treated CD45.1$^+$/CD45.2$^+$ spleen transplantation mice. (B) Clustering 8064 monocytes/macrophages (Monos) from different samples. Uniform Manifold Approximation and Projection (UMAP) plots display single-cell RNA sequencing data with annotated clusters. (C) Cell count and cell percentage of each Mono cell cluster of the five samples. (D) Annotation of pseudotemporal dynamics among Mono clusters (left). Pseudotemporal trajectory and directionality among Mono clusters revealed by RNA velocity (right). (E) Gene expression patterns of Spn2, Treml4, Cx3cr1, Ly6c2, and Ccr2 among Mono clusters. (F) Violin plots of relative marker gene expressions of Mono-3 (sM-2) and Mono-5 (sMφ). i.p., intraperitoneal; SP, spleen.

cells from both donors showed advantageous migration to SP$^-$ recipients, but only cells from CCl_4-treated donor mice showed advantageous migration to CCl_4-treated SP$^-$ recipients (Figure 3C). Migration of splenic CD11b$^+$ cells to other organs showed no significant difference (Figure 3D). These data demonstrate that splenic CD11b$^+$ cell migration to livers account for the role of the spleen in facilitating intrahepatic Ly6C^{lo} MoMF accumulation and exacerbating liver fibrosis progression.

Splenic CD11b$^+$ cells are visualized to accumulate intrahepatically in mice with liver fibrosis

To obtain in vivo evidence for splenic cells migration to liver, we used photoconvertible KikGR transgenic mice.[43] Upon site-specific irradiation at 405 nm, KikGreen splenic cells were converted into KikRed (Figure 4A) and discovered in the liver within 24 h (Figure 4B). Increased migration of KikRed splenic cells into livers was observed in mice treated with CCl_4 (Figure 4D). Furthermore, in the short-term spleen transplantation, there were also more CD45.1$^+$ splenic cells, especially CD45.1$^+$CD11b$^+$ cells, detected in livers of CD45.2$^+$ mice that received spleens from a CCl_4-treated CD45.1$^+$ donor (Figure 4D).

To observe long-term (LT) maintenance of spleen-derived CD11b$^+$ cells in the liver, we traced splenic cell distribution in vivo for a 6-week duration. The results also showed more abundant CD45.1$^+$CD11b$^+$ cells in livers of recipient mice treated with CCl_4 (Figure 4E). The results were further confirmed in KikGR/wild-type LT spleen transplantation (Figure S2A). Besides, we observed an increased distribution of CD45.1$^+$CD11b$^+$ cells in peripheral blood (Figure 4F), suggesting the active mobilization of splenic cells upon liver fibrosis. These data provide solid evidence for the migration and accumulation of spleen-derived CD11b$^+$ cells in fibrotic livers.

Spleen-derived monocytes-1 as a specific subtype from splenic CD11b$^+$ cells are identified in fibrotic liver

To depict the unique characteristics of these specially accumulated splenic CD11b$^+$ cells, CD45.1$^+$CD11b$^+$ cells were isolated from livers of CCl_4-treated CD45.1$^+$/CD45.2$^+$ spleen transplantation mice (fibrotic spleen-derived myeloid cells; FSDMs) and profiled with scRNA-seq. Similarly, CD11b$^+$ cells from spleens or livers of Oil- or CCl_4-treated mice, respectively, were also profiled (Figure 5A). Based on graph-based clustering and known marker expression, 27 immune cell clusters across nine lineages were identified, among which monocytes/macrophages (Monos) and neutrophils accounted for the major groups (Figure S3A, B). Each lineage was denoted by their unique signature genes (Figure S3C). Quality control metrics were highly reproducible among individual samples and conditions (Figure S4 and Supporting Materials S1 and S2).

Among the sequenced cells, Monos showed an obvious enrichment in FSDMs and a striking heterogeneity in livers (Figure 5B, Figure S3). The 8064 Monos from the five samples revealed five clusters. Mono-2 showed expansion in both splenic and hepatic Monos of CCl_4-treated mice and was the dominant population of Monos in FSDMs. Mono-3 and Mono-4 were enriched in FSDMs and CCl_4-treated livers but not present in spleens. Mono-5 was abundant only in FSDMs but slightly present in other samples. Mono-1 was also a large Mono subpopulation but showed no dominance in the liver and spleen of CCl_4-treated mice (Figure 5B). These differences were validated by quantification of cell counts and cell percentages (Figure 5C).

After that, the sequential relationship of the Mono clusters was realized by mapping them along a pseudotemporal trajectory, and their directionality was interrogated via spliced and unspliced mRNA ratios.[44] Both results suggested the sequential relationship of "Mono-2–Mono-4–Mono-3–Mono-5" (Figure 5D). We assumed Mono-2 to be the initial spleen-derived population that migrated to fibrotic livers and named it as spleen-derived monocyte (sM)-1, named Mono-3 as sM-2, and considered Mono-4 as a neglected cluster for its small count. Specific signatures for Mono-2 were identified, among which *Spn* (encoding CD43 protein), *Treml4*, and *Cx3cr1* were highly expressed, and *Ly6c2* and *Ccr2* were lowly expressed (Figure 5E). Therefore, we defined sM-1s as CD11b$^+$ Ly6G$^-$CD43^{hi}Ly6C^{lo} cells. Genes highly expressed in Mono-3 (*Msr1*, *Clec4d*, *Mif*, *Cstb*) also showed impressive expression levels in Mono-5; however, Mono-5 specifically expressed the macrophage signature molecules such as the *Mertk, Adgre1*, *Fcgr1*,

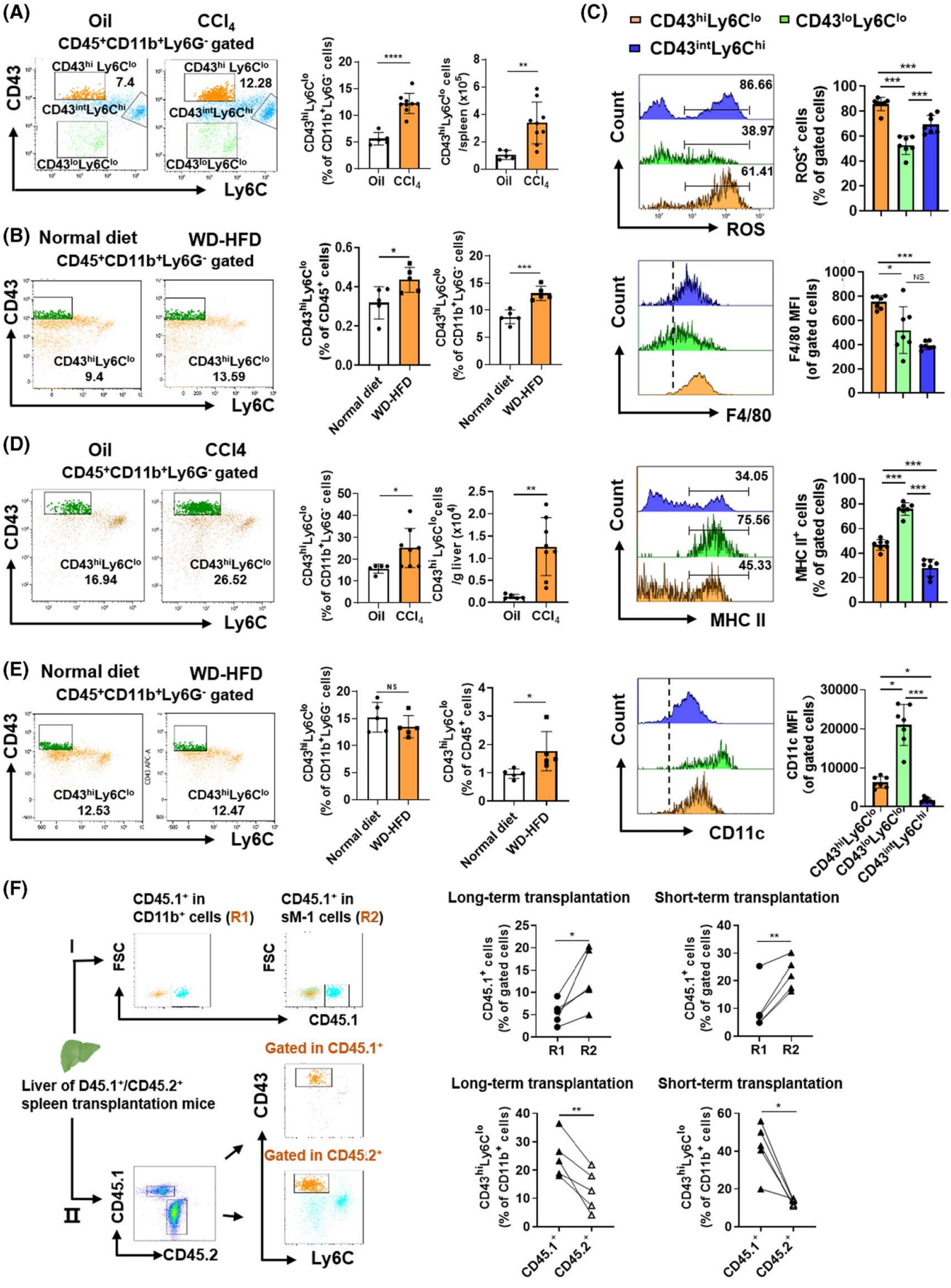
(A)
Oil
CCl4
CD45+CD11b+Ly6G- gated
CD43hi Ly6Clo
7.4
12.28
CD43intLy6Chi
CD43loLy6Clo
CD43
Ly6C
CD43hiLy6Clo (% of CD11b+Ly6G- cells)
CD43hiLy6Clo cells /spleen (x10^5)
Oil
CCl4
(B) Normal diet
WD-HFD
CD45+CD11b+Ly6G- gated
CD43hiLy6Clo
9.4
13.59
CD43hiLy6Clo (% of CD45+ cells)
CD43hiLy6Clo (% of CD11b+Ly6G- cells)
Normal diet
WD-HFD
(C)
CD43hiLy6Clo
CD43loLy6Clo
CD43intLy6Chi
Count
86.66
38.97
61.41
ROS
ROS+ cells (% of gated cells)
F4/80
F4/80 MFI (of gated cells)
NS
(D)
Oil
CCl4
CD45+CD11b+Ly6G- gated
CD43hiLy6Clo
16.94
26.52
CD43hiLy6Clo cells /g liver (x10^4)
34.05
75.56
45.33
MHC II
MHC II+ cells (% of gated cells)
(E) Normal diet
WD-HFD
CD45+CD11b+Ly6G- gated
CD43hiLy6Clo
12.53
12.47
CD43hiLy6Clo (% of CD45+ cells)
CD11c
CD11c MFI (of gated cells)
(F)
CD45.1+ in CD11b+ cells (R1)
CD45.1+ in sM-1 cells (R2)
FSC
CD45.1
Liver of D45.1+/CD45.2+ spleen transplantation mice
Gated in CD45.1+
Gated in CD45.2+
CD45.2
Long-term transplantation
Short-term transplantation
CD45.1+ cells (% of gated cells)
R1
R2
CD43hiLy6Clo (% of CD11b+ cells)
CD45.1+
CD45.2+

FIGURE 6 Splenic monocyte (sM)-1s marked with CD11b$^+$CD43^{hi}Ly6C^{lo} function in much mature status and prefer migrating into livers of fibrosis mice. (A) Representative cytometry for gating splenic CD11b$^+$CD43^{hi}Ly6C^{lo}, CD11b$^+$CD43^{int}Ly6C^{hi}, and CD11b$^+$CD43^{lo}Ly6C^{lo} cells of mice treated with oil or CCl_4. Frequencies and absolute numbers of splenic CD11b$^+$CD43^{hi}Ly6C^{lo} cells were then calculated. (B) Representative cytometry for gating splenic CD11b$^+$CD43^{hi}Ly6C^{lo} of mice fed with normal diet or Western high-fat diet (WD-HFD). Frequencies of splenic CD11b$^+$CD43^{hi}Ly6C^{lo} cells were then calculated. (C) Representative cytometry of ROS, F4/80, MHC II, and CD11c expression on different subtypes of splenic CD11b$^+$ cells. Percentages of ROS$^+$ and MHC II$^+$ cells and MFI of F4/80 and CD11c were then calculated. (D) Representative cytometry for gating hepatic CD11b$^+$CD43^{hi}Ly6C^{lo} cells of mice treated with oil or CCl_4. Frequencies and absolute numbers of the cells were then calculated. (E) Representative cytometry for gating hepatic CD11b$^+$CD43^{hi}Ly6C^{lo} cells of mice fed with normal diet or WD-HFD. Frequencies of hepatic CD11b$^+$CD43^{hi}Ly6C^{lo} cells were then calculated. (F) Frequencies of donor spleen-derived CD45.1$^+$ cells in hepatic CD11b$^+$CD43^{hi}Ly6C^{lo} or CD11b$^+$ cells, and CD11b$^+$CD43^{hi}Ly6C^{lo} cells in hepatic CD45.1$^+$ or CD45.2$^+$ cells of short-term and long-term CD45.1$^+$/CD45.2$^+$ spleen transplantation mice. Data are shown as the mean ± SEM. Mann–Whitney rank sum test and the Student's *t* test were performed for statistical significance. *, **, and *** stand for $p < 0.05$, <0.01, and <0.001, respectively. MFI, median fluorescence intensity; MHC II, major histocompatibility complex II; ROS, reactive oxygen species.

and *H2* family (Figure 5F). We named Mono-5 as spleen-derived macrophage (sMφ).

sM-1s marked with CD11b$^+$CD43^{hi}Ly6C^{lo} function in much mature status and prefer migrating into livers of mice with liver fibrosis

Flow cytometry analysis confirmed the expansion of CD11b$^+$Ly6G$^-$CD43^{hi}Ly6C^{lo}-gated sM-1s in spleens of CCl_4-treated (Figure 6A) and WD-HFD mice (Figure 6B). Consistent with the scRNA-seq data, the CD43^{hi}Ly6C^{lo} subpopulation of CD11b$^+$Ly6G$^-$ cells had the highest frequencies of both CX_3CR1^+ and TREML4$^+$ cells (Figure S5A, B), and these cells had a similar mRNA profile and pathway enrichment to Mono-2 in the scRNA-seq data (Figure S5C, D). Besides, CD43^{hi}Ly6C^{lo} cells had higher level of reactive oxygen species (ROS) production and lower levels of major histocompatibility complex II (MHC II) and CD11c expression, which was distinguished from the CD43^{lo}Ly6C^{lo} subpopulation but similar to the CD43^{int}Ly6C^{hi} subset. Additionally, CD43^{hi}Ly6C^{lo} cells expressed a high level of F4/80, indicating a much mature status (Figure 6C).

Expansion of sM-1s was also confirmed in livers of CCl_4-treated (Figure 6D) and WD-HFD mice (Figure 6E). The intrahepatic sM-1s had similar CX_3CR1, higher F4/80, and lower MHC II expression compared with their counterparts in the spleen (Figure S6). Within livers of the CCl_4-treated CD45.1$^+$/CD45.2$^+$ spleen transplantation mice, the frequency of CD45.1$^+$ spleen-derived cells in sM-1s was higher than that in CD11b$^+$ cells, and the proportion of sM-1s in CD45.1$^+$ cells was higher than that in CD45.2$^+$ cells (Figure 6F). These findings demonstrate preferential migration of splenic sM-1s into fibrotic livers.

sM-1s are trained to be pathogenic sM-2s and sMφs in fibrotic hepatic milieu

To study the intrahepatic development of the recruited sM-1s, splenic sM-1s were treated with fibrotic hepatocyte conditioned medium (liver-CM) to mimic their transformation in the hepatic environment. Compared with freshly sorted sM-1s, liver-CM–treated sM-1s had increased expressions of *Cstb*, *Mif*, *Msr1*, and *Clec4d* (Figure 7A), which were highly expressed in both sM-2 and sMφ. Liver-CM–treated sM-1s also had decreased ROS production (Figure 7B), decreased MHC II, and slightly increased F4/80 (encoded by *Adgre1*) and Ly6C expressions (Figure 7C), and the changes in expressions of F4/80 and MHC II were similar with their differential expressions between liver and spleen sM-1s (Figure S6). Moreover, liver-CM–treated sM-1s had a more similar mRNA profile to sM-2 (Figure S7A) than that of sMφ (Figure S7B), indicating that liver-CM treatment has led to the transformation of sM-1 to sM-2, which might be a transitional state before transforming into sMφ. Cytokines highly expressed in the liver-CM of CCl_4-treated mice (IL-1α, IL-12, IL-13, and IL-6) may play important roles in supporting cell survival and promoting differentiation of monocyte to macrophage (Figure 7D, Figure S8).

We also determined the phenotypic transition of sM-1s in vivo. Freshly isolated splenic sM-1s were intrahepatically injected to Oil- or CCl_4-treated recipient mice (Figure 7E). There were more transferred cells observed in CCl_4-treated recipients (data not shown), and these cells gained a higher expression of CX_3CR1, F4/80, MHC II, and CD64 within livers of both recipients (Figure 7F, Figure S9). These alterations were consistent with the changes among sM-1 and sMφ (Figure 5F), further confirming the sequential development from sM-1 to sM-2 and then to sMφ.

To reveal the role of spleen-derived Monos in fibrotic liver, several genes related to macrophage-mediated HSC recruitment, activation, or survival were combined as a module for expression score analysis. The sM-2 possessed the highest expression of *Il1b*, *Tgfb1*, and *Vegfa*, sMφ possessed the highest expression of *Tnfa* and *Ccl3* (Figure S10A), and sM-2 and sMφ had a significantly higher score in this module (Figure S10B), prompting them to play crucial roles in activating HSCs. Accordingly, the HSC line *JS1* cocultured with liver-CM–treated sM-1s, but not freshly sorted ones, showed

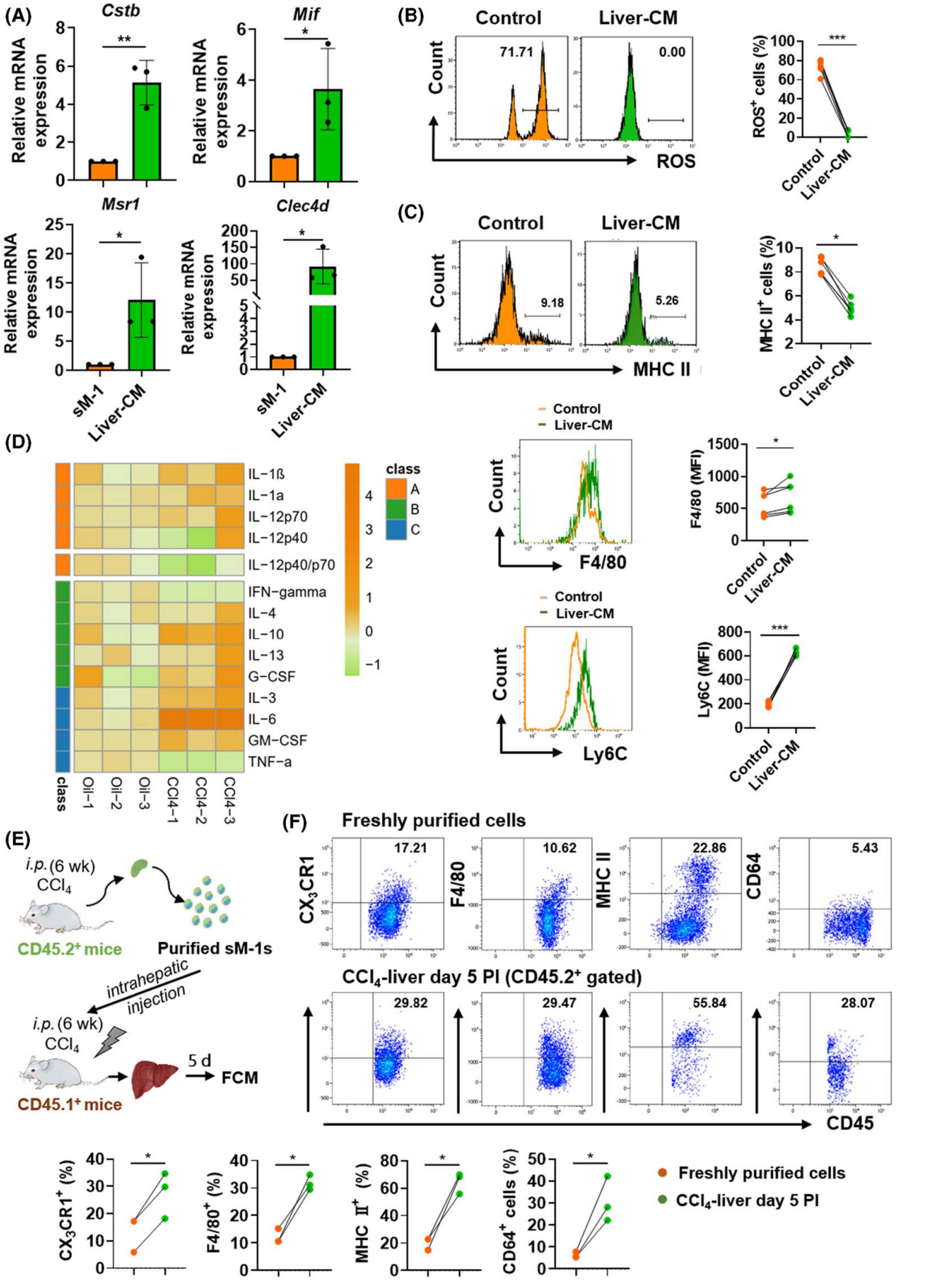
(A)
Cstb
Mif
Msr1
Clec4d
Relative mRNA expression
sM-1
Liver-CM
(B)
Control
Liver-CM
Count
71.71
0.00
ROS
ROS+ cells (%)
(C)
9.18
5.26
MHC II
MHC II+ cells (%)
(D)
IL-1ß
IL-1a
IL-12p70
IL-12p40
IL-12p40/p70
IFN-gamma
IL-4
IL-10
IL-13
G-CSF
IL-3
IL-6
GM-CSF
TNF-a
class
Oil-1
Oil-2
Oil-3
CCl4-1
CCl4-2
CCl4-3
F4/80
F4/80 (MFI)
Ly6C
Ly6C (MFI)
(E)
i.p. (6 wk) CCl4
CD45.2+ mice
Purified sM-1s
intrahepatic injection
CD45.1+ mice
5 d
FCM
(F)
Freshly purified cells
CX3CR1
F4/80
MHC II
CD64
17.21
10.62
22.86
5.43
CCl4-liver day 5 PI (CD45.2+ gated)
29.82
29.47
55.84
28.07
CD45
CX3CR1+ (%)
F4/80+ (%)
MHC II+ (%)
CD64+ cells (%)
Freshly purified cells
CCl4-liver day 5 PI

FIGURE 7 Spleen-derived monocyte (sM)-1 trained in fibrotic hepatic milieu gain sM-2 and spleen-derived macrophage (sMφ) features. (A) Indicated gene expression of freshly sorted sM-1s and fibrotic hepatocyte conditioned medium (liver-CM)–treated sM-1s analyzed by real time quantitative PCR (RT-qPCR). sM1, freshly sorted sM-1s; Liver-CM, liver-CM–treated sM-1s. (B) Representative cytometry of ROS expression on sM-1s treated with liver-CM or control complete medium (Control) for 24 h. Percentages of ROS^+ cells were then calculated. (C) Representative cytometry of MHC II, F4/80, and Ly6C expression on differentially treated sM-1s. Percentages of MHC II^+ cells and MFI of F4/80 and Ly6C on differentially treated cells was then calculated. (D) Cytokine expression profiles of liver-CM of Oil-treated mice (Oil) and CCl_4-treated mice (CCl_4) detected by Luminex. Class A, proinflammatory; Class B, anti-inflammatory; Class C, cell survival and macrophage differentiation. (E) Scheme of the in vivo training experiment. Primary sM-1s were sorted from spleens of CCl_4-treated $CD45.2^+$ mice and intrahepatically injected to CCl_4-treated $CD45.1^+$ mice. Features of freshly isolated sM1s and cells trained by the fibrotic hepatic milieu for 5 days were compared. (F) Representative cytometry of CX3CR1, F4/80, MHC II, and CD64 expression on freshly isolated sM-1s and intrahepatically trained cells. Percentages of $CX3CR1^+$, $F4/80^+$, MHC II^+, and $CD64^+$ cells were then calculated. Data are shown as the mean ± SEM. Student's *t* test was performed for the statistical significance. *, **, and *** stand for $p < 0.05$, <0.01, and <0.001, respectively. i.p., intraperitoneal; FCM, flow cytometry; MFI, median fluorescence intensity; MHC II, major histocompatibility complex II; ROS, reactive oxygen species.

increased expression of ECMs (Figure 8A). Transfusion of splenic sM-1s to CCl_4-treated splenectomy mice resulted in exacerbated liver fibrosis (Figure 8B,C) and increased $Ly6C^{lo}$ MoMF accumulation (Figure 8D). We also stained the human counterparts of sM-1 as $CD11b^+CD16^+CD43^+$ cells[45,46] and observed localization of these cells in close vicinity to the fibrotic region with high expression of collagen I (Figure 8E, Figure S11) in cirrhotic liver tissues.

DISCUSSION

The present study found that a unique subtype of $CD11b^+CD43^{hi}Ly6C^{lo}$ monocytes expands in spleens of mice with liver fibrosis. These cells are actively recruited to fibrotic liver and shift to macrophage phenotype, facilitate intrahepatic $Ly6C^{lo}$ MoMFs accumulation, and exacerbate liver fibrogenesis by activating HSCs. Our findings provide direct evidence that splenocytes migrate into the fibrotic liver and account for the pathogenic population, illustrating a partial sketch of the spleen–liver axis involvement in liver diseases.

The spleen and liver are both important components of portal circulation; influx of splenic blood into liver through the portal vein enables substance exchange and cell interflow between these two organs.[47] The spleen–liver axis has been proposed as playing roles in conditions including chronic liver disease[15,48] and metabolism.[16] However, the knowledge about the properties of the spleen–liver axis and the mechanism of the spleen–liver axis influencing liver pathological condition is very limited. Although the spleen has been suggested as acting as a source of profibrotic cytokines[18,49] or immune cells[6,7,24,50] to participate in the progression of chronic liver diseases, little direct evidence is provided. Our present study introduced diverse in vivo splenic cell-tracing models of spleen-specific photoconversion[43] and spleen transplantation. By virtue of these models, increased migration of splenic $CD11b^+$ cells to fibrotic livers was observed (Figure 4), and the intrahepatically located spleen-derived $CD11b^+$ cells were successfully isolated for further characterization

Generally, two different subsets of monocytes exist in mice.[51,52] Classical monocytes marked with $Ly6C^{hi}CCR2^{hi}CX_3CR1^{lo}$ are "vanguards" that originate from bone marrow and rapidly respond to inflammatory signals.[53] Nonclassical monocytes marked with $Ly6C^{lo}CCR2^{lo}CX_3CR1^{hi}$ with ambiguous sources rarely immigrate into peripheral tissues but abundantly patrol along blood vessel endothelia and extravasate into tissues during an inflammatory response.[54,55] In our study, spleen-derived $CD11b^+$ cells isolated from fibrotic livers were annotated by scRNA-seq, and a subtype of monocytes (sM-1s) marked with $CD11b^+CD43^{hi}Ly6C^{lo}$ was identified. The sM-1s were characterized with "nonclassical"-like phenotype of high CX_3CR1 expression but low CCR2 and Ly6C expression (Figure 5). Generally, $Ly6C^{hi}$ monocytes as vital effector cells are actively mobilized to peripheral tissues where they downregulate Ly6C expression and differentiate into macrophages.[9,56,57] $Ly6C^{lo}$ monocytes are supposed to be a mature monocyte subtype and have longer half-life.[58,59] Consistently, in our study, sM-1s present a much mature status with higher expression of F4/80 than the $Ly6C^{hi}$ subpopulation. However, the cells also have a similar high production of ROS with $Ly6C^{hi}$ subtype, indicating that they might be in the effector state. Although there have been reports of $Ly6C^{lo}$ monocytes differentiating into inflammatory macrophages,[60] they are more likely to function by inducing the differentiation of $Ly6C^{hi}$ monocytes,[61] helping recruit active immune cells,[62] or secreting growth factors.[63,64]

The sequential relationship analysis in the present study revealed a sequential development of sM-1 to sM-2, which gained higher expressions of *Cstb*, *Mif*, *Msr1*, and *Clec4d* and enhanced cytokine activity, and then to sMφ, which gained expressions of macrophage function–associated molecules like MERTK,[65] F4/80, and CD64[27,66] (Figure 7, Figures S7 and S10). Nonetheless, the in vitro induced "sM-2" in our system also had some characteristics of sMφ (e.g., increased F4/80), so we thought that sM-2 might be a transition

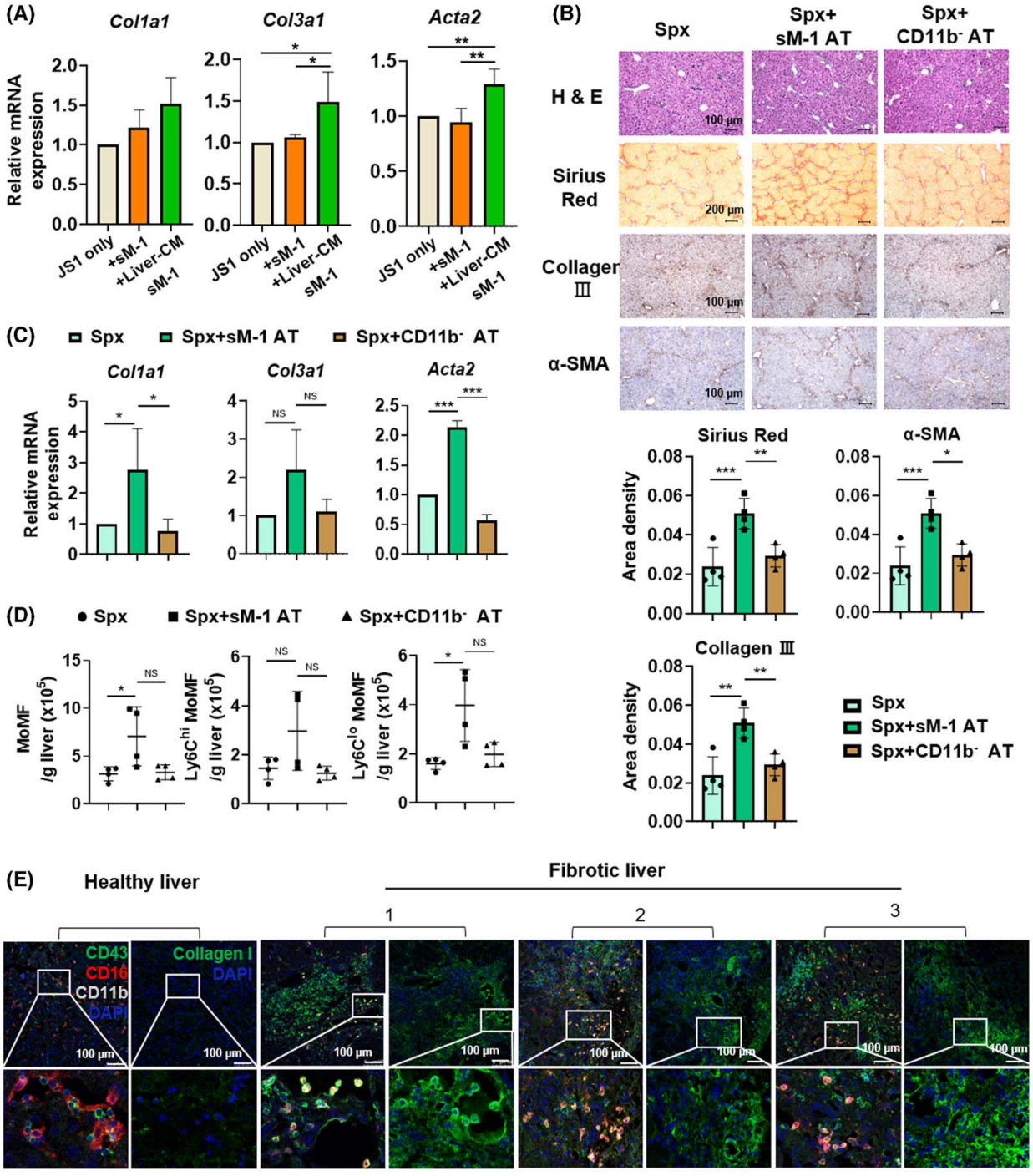

FIGURE 8 Spleen-derived monocyte (sM)-2s and spleen-derived macrophages (sMφs) derived from sM-1s promote liver fibrosis. (A) Expression of hallmark genes for hepatic stellate cell (HSC) activation analyzed by real time quantitative PCR (RT-qPCR) after coculture with freshly sorted or fibrotic hepatocyte conditioned medium (liver-CM)–treated sM-1s. sM-1, freshly sorted sM-1s; Liver-CM sM-1, liver-CM–treated sM-1s. (B) Representative histological images of hematoxylin and eosin (H&E), Sirius Red, collagen III, and α-SMA staining in formalin-fixed and paraffin-embedded liver tissue, and quantification of positive area fraction. Scale bar, 100 μm (H&E, collagen III, and α-SMA) or 200 μm (Sirius Red). (C) Expression of hallmarker genes for HSC activation analyzed by RT-qPCR among mice that underwent different operations. (D) Absolute numbers of hepatic Ly6C^{hi} and Ly6C^{lo} monocyte-derived macrophages (MoMFs). (C–D) Male C57BL/6 mice intraperitoneally injected with CCl_4 for 6 weeks were splenectomized (Spx) and divided into three groups and received adoptive transfusion (AT) of splenic sM-1s or CD11b$^-$ cells 2 weeks after Spx (Spx+sM-1 AT or Spx+CD11b$^-$AT), respectively. (E) Representative immunofluorescence images of CD11b$^+$CD16$^+$CD43$^+$ cell and collagen I staining in optimal cutting temperature compound (O.C.T.)-embedded frozen liver tissue. The fibrotic livers were representative images of tissues from three patients with hepatitis B cirrhosis-related portal hypertension complicated with hypersplenism. Scale bar, 100 μm. Data are shown as the mean ± SEM. One-way analysis of variance (ANOVA) and multiple comparisons (LSD) after ANOVA were performed for the statistical significance. *, **, and *** stand for $p < 0.05$, <0.01, and <0.001, respectively.

state of sMφ. Unexpectedly, the similar transition was observed in sM-1s transfused to Oil-treated recipients, and this might be attributed to fewer sM-1s recruited to liver. After that, these transformed cells of both sM-2s and sMφs were verified to exacerbate liver fibrogenesis by activating HSCs. These results indicate that differentiation of sM-1s themselves into profibrotic macrophages might be a crucial means by which sM-1s participate in liver fibrosis. However, the profibrotic function of sM-1s and their "descendants" needs to be further confirmed by intervention like cell-specific depletion. The potential factors for inducing splenic sM-1s expansion or mediating their intrahepatic transformation have been preliminarily explored, but more details remain to be elucidated. Moreover, the existence of sM-1s in NAFLD mice and in patients with cirrhotic portal hypertension has been verified, and it would be interesting to investigate the contribution of these cells to fibrogenesis in clinical liver diseases and rodent models closer to human liver diseases.

Identification of the $CD11b^{+}CD43^{hi}Ly6C^{lo}$ monocyte subset might provide a therapeutic strategy for chronic liver disease by targeting unique cells in the spleen rather than splenectomy. Antagonists against the chemokine receptor CCR2 have shown promising effects in ameliorating liver injury through inhibiting $Ly6C^{hi}$ monocyte recruitment.[53,54,67] CD43 appears to function by antiadhesion[68,69] and suppressing activation[70] in immune cells. Thus, we make the hypothesis that the high expression level of CD43 on sM-1s might facilitate their emigration from spleen to liver, and the following downregulation of CD43 in liver might promote their maturation. Therefore, our present study highlights CD43 as a potential therapeutic target. CX_3CR1 is highly expressed on sM-1s, and the CX_3CR1 antagonist has been proven a potent inhibitor of atherosclerotic lesions progression.[71] Targeted interruption of the spleen–liver axis while preserving other physiological functions of the spleen, for example, by blocking CD43 and CX_3CR1, might be effective for clinical practice.

In summary, our work describes a subtype of splenic monocytes that preferentially migrate into fibrotic liver, shift to macrophage phenotype, and function as the pathogenic population in fibrogenesis by activating HSCs. Our findings propose an attractive mode of the spleen–liver axis involved in liver disease and indicate a particular process of spleen-derived monocytes developing into pathogenic macrophages in the liver. Identifying the features of the distinct spleen-derived Monos and signals that instructing the recruitment and transition of these cells may provide strategies for chronic liver disease therapy by targeting the source.

AUTHOR CONTRIBUTIONS

Shaoying Zhang and Dan Wan performed most of the experiments. Mengchen Zhu and Chongyu Zhang performed the animal surgery like splenectomy and spleen transplantation. Guihu Wang and Na Huang performed the immune-histochemical experiments. Xurui Zhang performed the photoconversion assay. Qi Shang, Chen Zhang, and Xi Liu helped with cell sorting and flow cytometry. Chunyan Zhang and Fanfan Liang helped with mouse breeding and genotyping. Jing Geng drew the graphical abstract. Guangyao Kong and Libo Yao helped interpret the data. Shaoying Zhang, Shemin Lu, and Yongyan Chen generated the figures and wrote the manuscript. Zongfang Li designed and supervised the study. All authors discussed the results and approved the manuscript.

ACKNOWLEDGMENTS

We thank Zhigang Tian (University of Science and Technology of China) for meaningful discussions, Liesu Meng (Xi'an Jiaotong University) for technical assistance, Jinsheng Guo (Zhongshan Hospital of Fudan University) for providing the murine HSC line *JS1* as a gift, and Xiaolong Qi (Zhongda Hospital of Southeast University) for suggestions on article submission. We thank CHESS-Shaanxi consortium for the coordinaion for this study.

FUNDING INFORMATION

This work was funded by the National Natural Science Foundation of China (no. 91842307 and 82173207 to Zongfang Li, no. 82101915 to Shaoying Zhang, no. 81922003 to Guangyao Kong), the Innovation Capacity Support Plan of Shaanxi Province (no. S2020-ZC-GHJD-0012 to Zongfang Li), and the Natural Science Foundation of Shaanxi Province (no. 2019JQ-970 to Shaoying Zhang).

CONFLICT OF INTEREST

The authors declare no competing interests.

DATA AVAILABILITY STATEMENT

All raw sequencing data have been deposited in the Sequence Read Archive (SRA) database under accession PRJNA885980 for the scRNA seq data and PRJNA884853 for the bulk mRNA seq data.

REFERENCES

1. Lee YA, Wallace MC, Friedman SL. Pathobiology of liver fibrosis: a translational success story. Gut. 2015;64:830–41.
2. Seki E, Schwabe RF. Hepatic inflammation and fibrosis: functional links and key pathways. Hepatology. 2015;61:1066–79.
3. Ramakrishna G, Rastogi A, Trehanpati N, Sen B, Khosla R, Sarin SK. From cirrhosis to hepatocellular carcinoma: new molecular insights on inflammation and cellular senescence. Liver Cancer. 2013;2:367–83.
4. Robinson MW, Harmon C, O'Farrelly C. Liver immunology and its role in inflammation and homeostasis. Cell Mol Immunol. 2016;13:267–76.
5. Tsuchida T, Friedman SL. Mechanisms of hepatic stellate cell activation. Nat Rev Gastroenterol Hepatol. 2017;14:397–411.
6. Romano A, Hou X, Sertorio M, Dessein H, Cabantous S, Oliveira P, et al. FOXP3+ regulatory T cells in hepatic fibrosis and

splenomegaly caused by *Schistosoma japonicum*: the spleen may be a major source of tregs in subjects with splenomegaly. PLoS Negl Trop Dis. 2016;10:e0004306.
7. Tanabe K, Taura K, Koyama Y, Yamamoto G, Nishio T, Okuda Y, et al. Migration of splenic lymphocytes promotes liver fibrosis through modification of T helper cytokine balance in mice. J Gastroenterol. 2015;50:1054–68.
8. Wu C, Ning H, Liu M, Lin J, Luo S, Zhu W, et al. Spleen mediates a distinct hematopoietic progenitor response supporting tumor-promoting myelopoiesis. J Clin Invest. 2018;128:3425–38.
9. Ramachandran P, Pellicoro A, Vernon MA, Boulter L, Aucott RL, Ali A, et al. Differential Ly-6C expression identifies the recruited macrophage phenotype, which orchestrates the regression of murine liver fibrosis. Proc Natl Acad Sci U S A. 2012;109: E3186–95.
10. Zheng CJ, Huang H, Xiao BH, Li T, Wang W, Wáng YXJ. Spleen in viral hepatitis-B liver fibrosis patients may have a reduced level of per unit micro-circulation: non-invasive diffusion MRI evidence with a surrogate marker. SLAS Technol. 2022;27:187–94.
11. Reiberger T. The value of liver and spleen stiffness for evaluation of portal hypertension in compensated cirrhosis. Hepatol Commun. 2021;6:950–64.
12. Lv X, Yang F, Guo X, Yang T, Zhou T, Dong X, et al. Hypersplenism is correlated with increased risk of hepatocellular carcinoma in patients with post-hepatitis cirrhosis. Tumour Biol. 2016;37:8889–900.
13. Nomura Y, Kage M, Ogata T, Kondou R, Kinoshita H, Ohshima K, et al. Influence of splenectomy in patients with liver cirrhosis and hypersplenism. Hepatol Res. 2014;44:E100–9.
14. Kedia S, Goyal R, Mangla V, Kumar A, S S, Das P, et al. Splenectomy in cirrhosis with hypersplenism: improvement in cytopenias, child's status and institution of specific treatment for hepatitis C with success. Ann Hepatol. 2012;11:921–9.
15. Tarantino G, Citro V, Balsano C. Liver-spleen axis in non-alcoholic fatty liver disease. Expert Rev Gastroenterol Hepatol. 2021;15:759–69.
16. Savastano S, Di Somma C, Pizza G, De Rosa A, Nedi V, Rossi A, et al. Liver-spleen axis, insulin-like growth factor-(IGF)-I axis and fat mass in overweight/obese females. J Transl Med. 2011; 9:136.
17. Keramida G, Dunford A, Kaya G, Anagnostopoulos CD, Peters AM. Hepato-splenic axis: hepatic and splenic metabolic activities are linked. Am J Nucl Med Mol Imaging. 2018;8:228–38.
18. Akahoshi T, Hashizume M, Tanoue K, Shimabukuro R, Gotoh N, Tomikawa M, et al. Role of the spleen in liver fibrosis in rats may be mediated by transforming growth factor beta-1. J Gastroenterol Hepatol. 2002;17:59–65.
19. Gotoh K, Inoue M, Masaki T, Chiba S, Shimasaki T, Ando H, et al. A novel anti-inflammatory role for spleen-derived interleukin-10 in obesity-induced inflammation in white adipose tissue and liver. Diabetes. 2012;61:1994–2003.
20. Sukhumavasi W, Kaewamatawong T, Somboonpoonpol N, Jiratanh M, Wattanamethanont J, Kaewthamasorn M, et al. Liver- and spleen-specific immune responses in experimental leishmania martiniquensis infection in BALB/c mice. Front Vet Sci. 2021;8:794024.
21. Li L, Wei W, Li Z, Chen H, Li Y, Jiang W, et al. The spleen promotes the secretion of CCL2 and supports an M1 dominant phenotype in hepatic macrophages during liver fibrosis. Cell Physiol Biochem. 2018;51:557–74.
22. Aoyama T, Kuwahara-Arai K, Uchiyama A, Kon K, Okubo H, Yamashina S, et al. Spleen-derived lipocalin-2 in the portal vein regulates Kupffer cells activation and attenuates the development of liver fibrosis in mice. Lab Invest. 2017;97:890–902.
23. Fonseca MT, Moretti EH, Marques LMM, Machado BF, Brito CF, Guedes JT, et al. A leukotriene-dependent spleen-liver axis drives TNF production in systemic inflammation. Sci Signal. 2021;14:eabb0969.
24. Yada A, Iimuro Y, Uyama N, Uda Y, Okada T, Fujimoto J. Splenectomy attenuates murine liver fibrosis with hypersplenism stimulating hepatic accumulation of Ly-6C(lo) macrophages. J Hepatol. 2015;63:905–16.
25. Karlmark KR, Weiskirchen R, Zimmermann HW, Gassler N, Ginhoux F, Weber C, et al. Hepatic recruitment of the inflammatory Gr1+ monocyte subset upon liver injury promotes hepatic fibrosis. Hepatology. 2009;50:261–74.
26. Zigmond E, Samia-Grinberg S, Pasmanik-Chor M, Brazowski E, Shibolet O, Halpern Z, et al. Infiltrating monocyte-derived macrophages and resident kupffer cells display different ontogeny and functions in acute liver injury. J Immunol. 2014;193: 344–53.
27. Wen Y, Lambrecht J, Ju C, Tacke F. Hepatic macrophages in liver homeostasis and diseases-diversity, plasticity and therapeutic opportunities. Cell Mol Immunol. 2021;18:45–56.
28. Xu J, Chi F, Guo T, Punj V, Lee WN, French SW, et al. NOTCH reprograms mitochondrial metabolism for proinflammatory macrophage activation. J Clin Invest. 2015;125:1579–90.
29. Mossanen JC, Krenkel O, Ergen C, Govaere O, Liepelt A, Puengel T, et al. Chemokine (C-C motif) receptor 2-positive monocytes aggravate the early phase of acetaminophen-induced acute liver injury. Hepatology. 2016;64:1667–82.
30. Yu X, Lan P, Hou X, Han Q, Lu N, Li T, et al. HBV inhibits LPS-induced NLRP3 inflammasome activation and IL-1β production via suppressing the NF-κB pathway and ROS production. J Hepatol. 2017;66:693–702.
31. Wehr A, Baeck C, Heymann F, Niemietz PM, Hammerich L, Martin C, et al. Chemokine receptor CXCR6-dependent hepatic NK T Cell accumulation promotes inflammation and liver fibrosis. J Immunol. 2013;190:5226–36.
32. Xia C, Razavi M, Rao X, Braunstein Z, Mao H, Toomey AC, et al. MRP14 enhances the ability of macrophage to recruit T cells and promotes obesity-induced insulin resistance. Int J Obes (Lond). 2019;43:2434–47.
33. Baeck C, Wehr A, Karlmark KR, Heymann F, Vucur M, Gassler N, et al. Pharmacological inhibition of the chemokine CCL2 (MCP-1) diminishes liver macrophage infiltration and steatohepatitis in chronic hepatic injury. Gut. 2012;61:416–26.
34. Tacke F. Targeting hepatic macrophages to treat liver diseases. J Hepatol. 2017;66:1300–12.
35. Luis TC, Killmann NM, Staal FJ. Signal transduction pathways regulating hematopoietic stem cell biology: introduction to a series of Spotlight Reviews. Leukemia. 2012;26:86–90.
36. Swirski FK, Nahrendorf M, Etzrodt M, Wildgruber M, Cortez-Retamozo V, Panizzi P, et al. Identification of splenic reservoir monocytes and their deployment to inflammatory sites. Science. 2009;325:612–6.
37. Van der Laan AM, Ter Horst EN, Delewi R, Begieneman MP, Krijnen PA, Hirsch A, et al. Monocyte subset accumulation in the human heart following acute myocardial infarction and the role of the spleen as monocyte reservoir. Eur Heart J. 2014;35: 376–85.
38. Robbins CS, Chudnovskiy A, Rauch PJ, Figueiredo JL, Iwamoto Y, Gorbatov R, et al. Extramedullary hematopoiesis generates Ly-6C(high) monocytes that infiltrate atherosclerotic lesions. Circulation. 2012;125:364–74.
39. Kim E, Yang J, Beltran CD, Cho S. Role of spleen-derived monocytes/macrophages in acute ischemic brain injury. J Cereb Blood Flow Metab. 2014;34:1411–9.
40. Wu W, Zhang J, Yang W, Hu B, Fallon MB. Role of splenic reservoir monocytes in pulmonary vascular monocyte accumulation in experimental hepatopulmonary syndrome. J Gastroenterol Hepatol. 2016;31:1888–94.
41. Guo J, Loke J, Zheng F, Hong F, Yea S, Fukata M, et al. Functional linkage of cirrhosis-predictive single nucleotide polymorphisms of Toll-like receptor 4 to hepatic stellate cell responses. Hepatology. 2009;49:960–8.

42. Zhang Z, Lin C, Peng L, Ouyang Y, Cao Y, Wang J, et al. High mobility group box 1 activates Toll like receptor 4 signaling in hepatic stellate cells. Life Sci. 2012;91:207–12.
43. Nowotschin S, Hadjantonakis AK. Use of KikGR a photo-convertible green-to-red fluorescent protein for cell labeling and lineage analysis in ES cells and mouse embryos. BMC Dev Biol. 2009;9:49.
44. La Manno G, Soldatov R, Zeisel A, Braun E, Hochgerner H, Petukhov V, et al. RNA velocity of single cells. Nature. 2018;560: 494–8.
45. Peng A, Ke P, Zhao R, Lu X, Zhang C, Huang X, et al. Elevated circulating CD14(low)CD16(+) monocyte subset in primary biliary cirrhosis correlates with liver injury and promotes Th1 polarization. Clin Exp Med. 2016;16:511–21.
46. Kunzmann LK, Schoknecht T, Poch T, Henze L, Stein S, Kriz M, et al. Monocytes as potential mediators of pathogen-induced T-helper 17 differentiation in patients with primary sclerosing cholangitis (PSC). Hepatology. 2020;72:1310–26.
47. Li L, Duan M, Chen W, Jiang A, Li X, Yang J, et al. The spleen in liver cirrhosis: revisiting an old enemy with novel targets. J Transl Med. 2017;15:111.
48. Tsushima Y, Endo K. Spleen enlargement in patients with nonalcoholic fatty liver: correlation between degree of fatty infiltration in liver and size of spleen. Dig Dis Sci. 2000;45:196–200.
49. Asanoma M, Ikemoto T, Mori H, Utsunomiya T, Imura S, Morine Y, et al. Cytokine expression in spleen affects progression of liver cirrhosis through liver-spleen cross-talk. Hepatol Res. 2014; 44:1217–23.
50. Wu L, Parekh VV, Hsiao J, Kitamura D, Van Kaer L. Spleen supports a pool of innate-like B cells in white adipose tissue that protects against obesity-associated insulin resistance. Proc Natl Acad Sci U S A. 2014;111:E4638–47.
51. Geissmann F, Jung S, Littman DR. Blood monocytes consist of two principal subsets with distinct migratory properties. Immunity. 2003;19:71–82.
52. Sunderkötter C, Nikolic T, Dillon MJ, Van Rooijen N, Stehling M, Drevets DA, et al. Subpopulations of mouse blood monocytes differ in maturation stage and inflammatory response. J Immunol. 2004;172:4410–7.
53. Heymann F, Trautwein C, Tacke F. Monocytes and macrophages as cellular targets in liver fibrosis. Inflamm Allergy Drug Targets. 2009;8:307–18.
54. Auffray C, Fogg D, Garfa M, Elain G, Join-Lambert O, Kayal S, et al. Monitoring of blood vessels and tissues by a population of monocytes with patrolling behavior. Science. 2007;317:666–70.
55. Thomas G, Tacke R, Hedrick CC, Hanna RN. Nonclassical patrolling monocyte function in the vasculature. Arterioscler Thromb Vasc Biol. 2015;35:1306–16.
56. Geissmann F, Manz MG, Jung S, Sieweke MH, Merad M, Ley K. Development of monocytes, macrophages, and dendritic cells. Science. 2010;327:656–61.
57. David BA, Rezende RM, Antunes MM, Santos MM, Freitas Lopes MA, Diniz AB, et al. Combination of mass cytometry and imaging analysis reveals origin, location, and functional repopulation of liver myeloid cells in mice. Gastroenterology. 2016;151: 1176–91.
58. Yona S, Kim KW, Wolf Y, Mildner A, Varol D, Breker M, et al. Fate mapping reveals origins and dynamics of monocytes and tissue macrophages under homeostasis. Immunity. 2013;38: 79–91.
59. Yang Q, Wang Y, Pei G, Deng X, Jiang H, Wu J, et al. Bone marrow-derived Ly6C(−) macrophages promote ischemia-induced chronic kidney disease. Cell Death Dis. 2019;10: 291.
60. Misharin AV, Cuda CM, Saber R, Turner JD, Gierut AK, Haines GK 3rd, et al. Nonclassical Ly6C(−) monocytes drive the development of inflammatory arthritis in mice. Cell Rep. 2014;9:591–604.
61. Morias Y, Abels C, Laoui D, Van Overmeire E, Guilliams M, Schouppe E, et al. Ly6C- monocytes regulate parasite-induced liver inflammation by inducing the differentiation of pathogenic Ly6C+ monocytes into macrophages. PLoS Pathog. 2015;11: e1004873.
62. Carlin LM, Stamatiades EG, Auffray C, Hanna RN, Glover L, Vizcay-Barrena G, et al. Nr4a1-dependent Ly6C(low) monocytes monitor endothelial cells and orchestrate their disposal. Cell. 2013;153:362–5.
63. Nahrendorf M, Swirski FK, Aikawa E, Stangenberg L, Wurdinger T, Figueiredo JL, et al. The healing myocardium sequentially mobilizes two monocyte subsets with divergent and complementary functions. J Exp Med. 2007;204:3037–47.
64. Schlitt A, Heine GH, Blankenberg S, Espinola-Klein C, Dopheide JF, Bickel C, et al. CD14+CD16+ monocytes in coronary artery disease and their relationship to serum TNF-alpha levels. Thromb Haemost. 2004;92:419–24.
65. Cai B, Dongiovanni P, Corey KE, Wang X, Shmarakov IO, Zheng Z, et al. Macrophage MerTK promotes liver fibrosis in nonalcoholic steatohepatitis. Cell Metab. 2020;31:406–21. e7.
66. Crane MJ, Daley JM, van Houtte O, Brancato SK, Henry WL Jr, Albina JE. The monocyte to macrophage transition in the murine sterile wound. PLoS One. 2014;9:e86660.
67. Friedman SL, Ratziu V, Harrison SA, Abdelmalek MF, Aithal GP, Caballeria J, et al. A randomized, placebo-controlled trial of cenicriviroc for treatment of nonalcoholic steatohepatitis with fibrosis. Hepatology. 2018;67:1754–67.
68. Ardman B, Sikorski MA, Staunton DE. CD43 interferes with T-lymphocyte adhesion. Proc Natl Acad Sci U S A. 1992;89: 5001–5.
69. Fukuoka M, Fukudome K, Yamashita Y, Tokushima M, Miyake K, Kimoto M. Antiadhesive function of 130-kd glycoform of CD43 expressed in CD4 T-lymphocyte clones and transfectant cell lines. Blood. 2000;96:4267–75.
70. Kyriakou D, Alexandrakis MG, Kyriakou ES, Liapi D, Kourelis TV, Mavromanolakis M, et al. Reduced CD43 expression on the neutrophils of MDS patients correlates with an activated phenotype of these cells. Int J Hematol. 2001;73: 483–91.
71. Poupel L, Boissonnas A, Hermand P, Dorgham K, Guyon E, Auvynet C, et al. Pharmacological inhibition of the chemokine receptor, CX3CR1, reduces atherosclerosis in mice. Arterioscler Thromb Vasc Biol. 2013;33:2297–305.

How to cite this article: Zhang S, Wan D, Zhu M, Wang G, Zhang X, Huang N, et al. $CD11b^{+}CD43^{hi}Ly6C^{lo}$ splenocyte-derived macrophages exacerbate liver fibrosis via spleen–liver axis. Hepatology. 2023;77:1612–1629. https://doi.org/10.1002/hep.32782